Large-scale ion generation for precipitation of atmospheric aerosols

Shaoxiang Ma [(a)][1], He Cheng[(a)][1], Jiacheng Li[1], Maoyuan Xu[1], Dawei Liu[1], and Kostya (Ken) Ostrikov[2]

[1]State Key Lab of Advanced Electromagnetic Engineering and Technology, School of Electronic and Electrical Engineering, Huazhong University of Science and Technology, WuHan, HuBei 430074, China

[2]Institute for Future Environments and School of Chemistry and Physics, Queensland University of Technology, Brisbane, Queensland 4000, Australia

[a] Equal contribution

Correspondence: Dawei Liu (liudw@hust.edu.cn)

Abstract. Artificial rain is explored as a remedy to climate change caused farmland drought and bushfires. Increasing the ion density in the open air is an efficient way to generate charged nuclei from atmospheric aerosols and induce precipitation or eliminate fog. Here we report on the development of the large commercial installation scale atmospheric ion generator based on corona plasma discharges, experimental monitoring and numerical modeling of the parameters and range of the atmospheric ions, and application of the generated ions to produce charged aerosols and induce precipitation at a scale of a large cloud chamber. The coverage area of the ions generated by the large corona discharge installation with the 7.2 km long wire electrode and applied voltage of -90 kV is studied under prevailing weather conditions including wind direction and speed. By synergizing over 300,000 localized corona discharge points, we demonstrate a substantial decrease of the decay of ions compared to a single corona discharge point in the open air, leading to a large-scale (30 m×23 m×90 m) ion coverage. Once aerosols combine with the generated ions, charged nuclei are produced.

The higher   wind speed has led to the larger areas covered by the plasma generated ions. The cloud chamber experiments (relative humidity $130\pm10\%$) suggest that the charged aerosols generated by ions with the density of $\sim 10^4/cm^3$ can accelerate the settlement of moisture by 38%. These results are promising for the development of large-scale installations for the effective localized control of atmospheric phenomena.

1. Introduction

The water cycle and rainfall on the Earth are affected by the climate change, causing widespread droughts around the world (Dai, 2013; Trenberth et al., 2014). Recently, more and more forest fires happened in North America, Australia and China. Besides that, the lack of water in many parts of Asia and Africa seriously influence the local agriculture, industry, and human health (Jolly et al., 2015; Lesk et al., 2016). The artificial rain has been used widely in many countries to alleviate the drought problems by enhancing precipitation. The artificial rain is commonly realized by dispersing substances, such as silver iodide, dry ice and table salts, which act as cloud condensation nuclei and alter the physico-chemical processes within the cloud.

It is well known that the ions generated by galactic cosmic rays in the atmosphere directly affect the changes in cloudiness of the Earth (Carslaw et al., 2002; Pierce and Adams, 2009). The experiment in the Wilson chamber suggested that ions generated by radioactive materials acted as condensation nuclei under supersaturation conditions (Yang et al., 2018). Nielsen *et al.* found that the charged nuclei could remain in the condensation phase even when the relative humidity is less than 100% (Nielsen et al., 2011). This is why plasma- and laser-based techniques have been employed to generate the charged nuclei in the open air to try to realize rain enhancement or, alternatively, fog elimination (Henin et al., 2009; Khain et al., 2004; Tan et al., 2016).

Ideally, the effects (e.g., precipitation of atmospheric aerosols) of the plasma-based methods should be delivered over the areas of small-to-medium-size farmlands. Indeed, it appears appealing to install, for example, a large-scale corona plasma discharge system on top of a hill and distribute the generated ions using the wind. Indeed, corona plasma discharges can release high-concentration ion fluxes, which can not only be transported to a large area by the upwind slope airflow, but also effectively interact with atmospheric aerosols thereby generating charged nuclei needed to induce or enhance water precipitation in the areas along the downwind direction. However, there are formidable science and technological challenges to implement it in practice. First, we are not aware of any systematic experimental and theoretical studies on the generation efficiency of ions, the

coverage area of ions and effect of wind on the ion transport at the relevant scale of the atmospheric ion generating installations. Second, the high efficiency of the ion generation in the laboratory does not necessarily translate into a similar performance at a scale. One reason is destructive interference of multiple corona discharges along the same plasma-generating wire, addressed in this work. Third, there are no reliable estimates of the volumes where the ions are generated at concentrations that are appropriate for atmospheric aerosol precipitation. Fourth, the reliable quantitative estimates of the significance of the effects of plasma-generated ions on moisture precipitation under real-world conditions are very limited, if available at all. Fifth, quantitative effects of the real-world wind on the ion coverage at the large installation scale are eagerly anticipated by the community.

In this work, we address all the above issues and report on the coverage area of ions generated by a large corona discharge system with the 7.2 km long wire electrode and applied voltage of -90 kV. The vertical and horizontal distribution of the ions in the downwind are measured under realistic weather conditions. The numerical models of the corona discharge and ion transport are developed. The results of numerical modelling are consistent with the experiment results, and indicates that the ions produced by the plasma discharge device may affect aerosol precipitation over large areas depending on the direction and speed of the wind. The effects of the plasma generated ions on moisture precipitation are studied experimentally at a scale of a large cloud chamber.

2. Methods

2.1 Corona discharge installation and ion measurements

Both the positive and negative corona discharge can be used to increase the ion density in the open air. Under the similar conditions of the electric circuit the loss of the positive corona is greater than that of negative corona at the same applied voltage. Because the negative corona curve is flatter and since larger negative corona currents can be obtained, the negative corona is much better adapted for the application such as fog elimination and electrical precipitation than the positive corona.(Sawant et al., 2012; Strong, 1913)

4

The wire electrode is a low cost and high efficiency plasma source configuration, especially for the large scale corona discharge system. For the wire electrode radius within the range of 100 μm to 1000 μm, the plasma thickness increases with increasing wire radius. The larger wires can generate more electrons, however, the electron energy decreases due to the lower electric field near the larger wire(Chen and Davidson, 2003). Stainless steel stranded wire is suitable wire electrode material considering durability and stability.

Electrons generated by negative corona discharge attach to electronegative gas molecules (such as, O_2) to generate negative ions (O_2^-). Recombination of electrons with positive ions is negligible. Therefore, ionization competes primarily with electron attachment. The ionization predominates over the electron attachment and new electrons are generated. The rate of ionization balances the rate of electron attachment at the reduced electric field of 120 Td (1 Td $=10^{-21}$ Vm^2). Beyond this ionization boundary, the attachment dominates over the ionization, and the electron density decrease gradually as the electric field decreases.(Chen and Davidson, 2003; Kossyi et al., 1992; Lowke and Morrow, 1994) In the region away from the electrode, because the absence of the electric field, the charged particles, including electrons and ions, perform a faster decay through the electron-ion and ion-ion recombination with background charged particles.(Xiong et al., 2010)

The large corona discharge system employed in this study has the floor area ~11304 m^2 (**Figure 1** (a) and (b)). Six poles each with the height of 20 m supporting the 7.2 km long wire electrode are erected vertically and arranged in a regular hexagon array. The wire electrodes are divided into two layers, at the height of 20 m and 15 m, i.e., with 5 m separation between the layers. There are 10 wire electrodes in each layer, and the horizontal distance between the wires is 50 cm to avoid the mutual interference. The stainless-steel wire has six strands and a diameter of 1 mm. The high voltage DC power supply is Technix 44-2015, which can monitor the output voltage and current value in real time.

Figure 1 (c) shows the satellite image of test zone. The hexagon shows the large-scale corona discharge system. The red points show the locations of the ion density measurements. The hydrogen

balloon carrying the ion counter (Air Ion Counter) is used to measure the vertical (5 m – 50 m) and horizontal (20 m – 50 m) ion density in the downwind as shown in Fig. 1(d). The horizontal distance between the hydrogen balloon measurement and the wire electrode is 20 m to ensure the safety of the experiment. The image of the corona discharge on the wire electrode is taken by digital camera Nikon D800 with the exposure time of 2 s. The optical emission spectroscopy (OES) of the negative corona discharge on the wire electrode with the applied voltage of -40 kV is measured by an optical spectrometer (Ocean optics USB4000+).

2.2 Ion transport model

The 2D numerical model is used to the study the distribution of ions within 1 m from the wire electrode. The model used in this study extends the existing models (He et al., 2013; Liu et al., 2012, 2014a, 2014b) to model the relevant phenomena at the relevant scales. The model solves the Poisson's equation and the transport equations for neutral and charged species as a function of time. The number density of each species is obtained by solving the continuity equation. The electric field is obtained by solving the Poisson's equation. The electron energy is calculated by the electron energy conservation equation.

The transient advection diffusion reaction equation (equation (1)) is used to study the effect of wind on the transport of ions (Albani et al., 2015; Ashrafi et al., 2017; Schleder and Martins, 2016)

$$\frac{\partial c}{\partial t} + u\nabla c = \nabla(K\nabla c) - \lambda c, \ c = c(x, y, z, t) \qquad , \qquad (1)$$

where c is the crosswind-integrated concentration of ions, t is time, u is the wind speed, $\nabla = (\frac{\partial}{\partial x}, \frac{\partial}{\partial y}, \frac{\partial}{\partial z})$, x is horizontal downwind direction, y is horizontal radial direction, z is vertical direction, and λ is the decay constant.

The eddy diffusion K represents the diffusion of ions under the influence of the turbulent state of atmosphere. During stable conditions, the maximum value of eddy diffusivity decreases with increasing stability. In stable conditions, a height at which turbulence maintained is limited by the

destruction of turbulent kinetic energy by negative buoyancy(Ulke, 2000), while in unstable conditions, the maximum value of eddy diffusivity increases with growing instability characterized by increasing values of H_A/L (H_A is the ABL-height, L is the Monin-Obukhov length).

The decay constant λ, it represents the decay of ions due to the recombination reactions between charged particles, such as $e+N_2^+{\rightarrow}N_2$, $e+O_2^+{\rightarrow}2O$, $O_2^-+N_2^++N_2{\rightarrow}2O+2N_2$, etc. According to our simulation results, the combination of numerous corona discharge points actually decreases the decay of ions generated by a single corona discharge point in the open air.

2.3 Cloud chamber experiments

The cloud chamber used to study the enhanced water condensation by ions has the size of 3 m×1.5 m×1.5 m (**Figure 2**). The temperature inside the chamber is 2±1°C during the experiment (Testo 605-H1). The dehumidifier (Gree DH40EF) and ultrasonic humidifier (Midea SC4E40) are used to control the humidity supersaturation at 130±10%. The laser illuminator (YGL01, planar laser source) is used to light up the cloud chamber. The changing process of droplets is recorded by the digital camera (Nikon D800) with a microscopic lens. Finally, an acceptor with the cross section of 10 cm² is placed at the bottom of the cloud chamber to accept the settlement of moisture.

3. Results and discussion

3.1 Corona discharges and ion generation

The applied voltage on the wire electrode with the length of 7.2 km is -90 kV (**Figure 1**), and the discharge current is 0.3 mA, so the plasma power is 27 W. **Figure 3** (b) shows that there are more than 20 corona discharge points on the wire electrode with the length of 1 m. Because the distance between the camera and the wire electrode is only 2 m, the applied voltage is therefore -40 kV to ensure the experimental safety. Although the six strands of stranded stainless-steel wire have good anti-stretching and anti-bending properties, there are numerous small peaks on the wires, which

help ignite corona discharges. Consequently, the minimum inception voltage of the corona discharge on the wire is only -15 kV. More corona discharge points are thus expected for the field experiment with the applied voltage of -90 kV.

Figure 3 shows the OES data of the corona discharge on the wire electrode. The brightest peaks can be seen around 315, 337, 350 and 380 nm, which are attributed to the nitrogen 2nd positive electronic transition ($N_2(C^3\Pi_u - B^3\Pi_g)$) and its family of vibrational rotational level sub-transitions (Antao et al., 2009; Hu et al., 2013; Wang et al., 2013; Zou et al., 2019). The OES of OH and O radicals are quite low compared with N_2 species(Gan et al., 2019).

For the negative corona discharge, the plasma region only occupies a very small portion of the space around the power electrode, negative ions occupy the region outside the plasma region (Chen and Davidson, 2003; Riba et al., 2018; Yao et al., 2019; Zhang et al., 2019). **Figure 4** (a) shows the boundary of the plasma region defined as the position where the reduced electric field (electric field divided by neutral density, E/N) of 80 Td (1 Td = 10^{-21} Vm^2) is 0.1 cm from the electrode (Chen and Davidson, 2003). Therefore, the negative ion density at the boundary of plasma region (~1cm from the electrode, reduced electric field ~10 Td) is chosen as the source density of negative ions for each case.

As the applied voltage amplitude increases from 30 kV to 90 kV, the source density at 1 cm from the single discharge point increases from $1.1\times10^8/cm^3$ to $3.9\times10^8/cm^3$, and the density at 1 m from the single discharge point increased from $1.8\times10^6/cm^3$ to $8\times10^6/cm^3$ (**Figure 4** (b)). In addition, **Figure 4** (c) suggests that the ion density in the whole simulation domain increases with the increasing applied voltage amplitude.

3.2 Ion transport

Figure 5 shows the effect of the wind on the transport of ions generated by a single corona discharge point. The ion density at the plasma boundary is chosen as the source density. The ion density measured at the position at 1 m from the electrode is consistent with the numerical result calculated

by Eq. (1). As the wind speed increases from 0 to 5.7 m/s, the ion density at 1 m increases from $2.5 \times 10^6/cm^3$ to $4 \times 10^6/cm^3$, and the density at 3 m increases from $3.2 \times 10^4/cm^3$ to $2 \times 10^5/cm^3$, which indicates that the diffusivity dominates the ions movement in the low electric field region, and the wind convection can substantially enhance the ion transport (Albani and Albani, 2019; Ashrafi et al., 2017; Hosseini and Stockie, 2016; Schleder and Martins, 2016).

Figure 6 (a) shows the coverage range (horizontal/vertical (x/z) direction) of negative ions generated by the large corona discharge system shown in **Figure 1**. In order to ensure the safety, the ion counter carried by the balloon starts recording the negative ion density at the position of 20 m from the wire electrode. The ion density decreases from $5 \times 10^5/cm^3$ to $8 \times 10^3/cm^3$ as the distance from the wire electrode increases from 20m to 30m. Afterwards, the ion density decreases to the background value as the horizontal distance increases to 40 m. The relatively high density $10^4/cm^3$ at the horizontal position of 50 m can be attributed to the random enhanced transport by gusts. The width of the coverage area in radial direction was 90 m. Therefore, the whole coverage volume was approximately 30 m (long) ×23 m (height) ×90 m (width). Aerosols can combine with the ions generated in this volume, thus creating a large number of charged nuclei within the volume (Anon, 2000; Bricard et al., 1968; Harrison, 2000; Harrison and Carslaw, 2003; Keefe et al., 1959).

It is interesting to note that the ion density at 20 m from the single corona discharge point is only $10^2/cm^3$ (**Figure 6** (c)), which is only 0.02% of the ion density generated by the large corona discharge system (**Figure 6** (a)). **Figure 3** (b) suggests the presence of more than 45 corona discharge points along the 1 m long wire electrode when the applied voltage is -40 kV, and the average distance between corona discharge points is only 2.5 cm. For the large corona discharge system with the 7.2 km long wire electrode and applied voltage of -90 kV, the number of the corona discharge points is expected to be at least 3.2×10^5 ($45 \times 7.2 \times 10^3$).

Figure 6 (d) shows the collective efficiency of ion transport of ions generated by the many corona discharge points. Because the distance between the corona discharge points is in the cm range and the coverage area of each corona discharge point is 25 m (x-direction) × 30m (y-direction) (**Figure 6**

(c)), the overlap of the coverage areas results in the high ion density in the open air.

The comparison between the experimental (**Figure 6** (a)) and simulation (**Figure 6** (c)) results suggest that the combination of numerous corona discharge points actually decreases the decay of ions generated by a single corona discharge point in the open air, and substantially increases the outward transport capacity of ions of the large corona discharge system. In the simulation model, by decreasing the decay constant λ by 4.533 times, the equation (1) provides a similar coverage area as measured in the experiment (compare **Figure 6** (a) and (b)).

Because the large corona discharge system may be setup on the mountain top, e.g., with an altitude of around 4,000 m (Farr and Chadwick, 2012; Mu et al., 2007; Shiyin et al., 2003; Zhou and Yang, 2010), the effect of the wind and applied voltage on the coverage area of large corona discharge system is also studied by the numerical model.

Figure 7 (a) – (c) suggest that as the wind speed increases from 2.89 m/s to 12.5 m/s, the axial length of the coverage area (ion density $\sim 10^4/cm^3$) increases from 26 m to 73 m. **Figure 7** (d) – (f) suggests that as the amplitude of the applied voltage increases from 60 kV to 180 kV, the axial length of the coverage area increases from 34 m to 46 m. The comparison between the effects of the wind and applied voltage indicates that the increasing transfer flux with the faster wind speed is a more efficient way to increase the coverage area of the large corona discharge system. The larger coverage area can facilitate the generation of charged nuclei, which eventually realize rain enhancement and fog elimination (Frederick and Tinsley, 2018; Tinsley and Zhou, 2015; Zhang et al., 2018a).

3.3 Ion-enhanced precipitation

The cloud chamber is used to study the enhancement of droplets growth by ions before the completion of the large-scale corona discharge system.   The corona discharge on the needle electrode (applied voltage of -23 kV) provides an environment with the ion density of $1.2 \times 10^5/cm^3 \sim 2 \times 10^4/cm^3$ in the cloud chamber, which corresponds to the ion density in the region $30 - 35$ m from the wire electrode (**Figure 6** (a)). The high ion density in the cloud chamber facilitates the aerosols

charging. Aerosols (diameter > 0.7μm) are mainly charged by the drift of ions on the electric field lines intersecting the surface of aerosols. The diffusion of ions to the surface of aerosols also contributes to the aerosols charging(Jidenko and Borra, 2012).

The size distribution of droplets of the natural settling case and the ion-enhanced settling case are compared in **Figure 8**. The droplet sizes are distributed mainly in the range of 10 ~ 40 μm for the case of natural settling. The charged aerosols are generated through the combination of ions and aerosols. Besides the conventional forces such as the thermophoretic and diffusophoretic forces, the electric forces contribute to the collisions between the small charged aerosols and uncharged aerosols. (Cherrier et al., 2017; Hashino et al., 2014; Luan et al., 2019; Roy et al., 2019; Wang and Pruppacher, 1977; Zhang et al., 2018b; Zhang and Tinsley, 2017). The charged aerosols can induce the image charge on large uncharged aerosols, and the consequent electric forces are the short range attractive force. The previous simulation results suggest that the charged aerosols can increase the collision rate between aerosols by 1 to 3 orders of magnitude(Tan et al., 2016). Therefore, the droplet sizes are distributed in the range of 50 - 80 μm for the case of charged aerosols settling case. However, the uncharged aerosols of the natural settling case (control group) can only cause limited increase of the particle size distribution. The large droplets generated by charged droplets can capture a large number of small aerosols during their settling process and cause faster settling of supersaturated water vapor in the cloud chamber. **Figure 8 (d)** indicates that the settling amount of moisture induced by charged aerosols is 38% higher than in the natural settling case (control group) at 10 min after the start of the experiment.

3.4 Technoeconomic estimates

As a simple techno-economic estimate, we note that the cost of the large corona discharge system including the DC power supply, 6 poles, the wires with length of 7.2 km was less than 250,000 Chinese Yuan (CNY). The low-maintenance solar and wind power system (estimated cost of 50,000 CNY) can provide a continuous supply of renewable energy for the corona plasma discharge system. This energy supply system can be installed on-site and operated off-the-grid. Even considering the

high construction cost of the system on the mid-altitude mountains to be about 200,000 CNY, the total cost of the installation was approximately 500,000 CNY. Importantly, this cost is well below the typical cost of a cloud seeding carried in China (at least 1 million CNY) to generate artificial rain. After the completion of the setup and real-world testing and optimization of the large-scale corona discharge installation, it may have an effect on the rainfall of downwind area. A similar approach can be used for fog elimination applications, for example along the airport runways. Importantly, the plasma system can be switched on to instantly generate the ions, and then switched off to also instantly cease the ion production whenever the wind direction or other atmospheric conditions change. This important feature of the plasma adds additional level of flexibility in commercial operation of the system.

4. Conclusion and implications

To summarize, a large-scale corona plasma discharge system was installed to analyze the production and the coverage area of negative ions that are capable to induce precipitation of atmospheric aerosols in downwind direction. The nitrogen species dominated the optical emission spectra of the negative corona discharges. The corona discharge was found to perform as a stable ion source with the density of $\sim 10^8/cm^3$. The coverage area of the ions was dramatically improved by using over 300,000 corona discharge points, which also reduced the common destructive interference leading to the decay of ion concentrations in the open air, thereby dramatically increasing the outward ion transport capacity of the large-scale corona plasma discharge installation. As a result, the large ion coverage area (30 m×23 m×90 m) has been achieved experimentally and validated by the numerical calculations. The faster wind speed was a more efficient way to increase the ion coverage area. The cloud chamber experiment confirms that the charged aerosols generated by ions can accelerate the settlement of moisture by 38%. These results indicate that the large scale corona discharge installation indeed can increase the ion density within a certain region. Furthermore, the ion-induced charged aerosols may realistically trigger water precipitation or, alternatively, fog elimination. Since the latter effects were studied using our large-scale cloud chamber laboratory system, systematic

field studies under real-world conditions are warranted to optimize the complex processes involved in ion-induced precipitation of atmospheric aerosols under prevailing weather conditions.

References

Albani, R. A. S. and Albani, V. V. L.: Tikhonov-type regularization and the finite element method applied to point source estimation in the atmosphere, Atmospheric Environment, 211, 69–78, doi:10.1016/j.atmosenv.2019.04.063, 2019.

Albani, R. A. S., Duda, F. P. and Pimentel, L. C. G.: On the modeling of atmospheric pollutant dispersion during a diurnal cycle: A finite element study, Atmospheric Environment, 118, 19–27, doi:10.1016/j.atmosenv.2015.07.036, 2015.

Anon: Estimation of the agglomeration coefficient of bipolar-charged aerosol particles, Journal of Electrostatics, 48(2), 93–101, doi:10.1016/S0304-3886(99)00053-4, 2000.

Antao, D. S., Staack, D. A., Fridman, A. and Farouk, B.: Atmospheric pressure dc corona discharges: operating regimes and potential applications, Plasma Sources Sci. Technol., 18(3), 035016, doi:10.1088/0963-0252/18/3/035016, 2009.

Ashrafi, K., Orkomi, A. A. and Motlagh, M. S.: Direct effect of atmospheric turbulence on plume rise in a neutral atmosphere, Atmospheric Pollution Research, 8(4), 640–651, doi:10.1016/j.apr.2017.01.001, 2017.

Bao, P., Lu, X., He, M. and Liu, D.: Kinetic Analysis of Delivery of Plasma Reactive Species Into Cells Immersed in Culture Media, IEEE Transactions on Plasma Science, PP(99), 1–9, doi:10.1109/TPS.2016.2578955, 2016.

Bricard, J., Billard, F. and Madelaine, G.: Formation and evolution of nuclei of condensation that appear in air initially free of aerosols, Journal of Geophysical Research (1896-1977), 73(14), 4487–4496, doi:10.1029/JB073i014p04487, 1968.

Carslaw, K. S., Harrison, R. G. and Kirkby, J.: Cosmic Rays, Clouds, and Climate, Science, 298(5599), 1732–1737,

doi:10.1126/science.1076964, 2002.

Chen, J. and Davidson, J. H.: Model of the Negative DC Corona Plasma: Comparison to the Positive DC Corona Plasma, Plasma Chemistry and Plasma Processing, 23(1), 83–102, doi:10.1023/A:1022468803203, 2003.

Cherrier, G., Belut, E., Gerardin, F., Tanière, A. and Rimbert, N.: Aerosol particles scavenging by a droplet: Microphysical modeling in the Greenfield gap, Atmospheric Environment, 166, 519–530, doi:10.1016/j.atmosenv.2017.07.052, 2017.

Dai, A.: Increasing drought under global warming in observations and models, Nature Clim Change, 3(1), 52–58, doi:10.1038/nclimate1633, 2013.

Dawei Liu, Iza, F. and Kong, M. G.: Evolution of the Light Emission Profile in Radio-Frequency Atmospheric Pressure Glow Discharges, Plasma Science, IEEE Transactions on DOI - 10.1109/TPS.2008.922426, 36(4), 952–953, 2008.

Farr, T. G. and Chadwick, O. A.: Geomorphic processes and remote sensing signatures of alluvial fans in the Kun Lun Mountains, China, Journal of Geophysical Research: Planets, 23091–23100, doi:10.1029/96JE01603@10.1002/(ISSN)2169-9100.SIRSAR1, 2012.

Frederick, J. E. and Tinsley, B. A.: The response of longwave radiation at the South Pole to electrical and magnetic variations: Links to meteorological generators and the solar wind, J. Atmos. Sol.-Terr. Phys., 179, 214–224, doi:10.1016/j.jastp.2018.08.003, 2018.

Gan, L., Duan, J., Zhang, S., Liu, X., Poorun, D., Liu, X., Lu, X., Duan, X., Liu, D. and Chen, H.: Cold atmospheric plasma ameliorates imiquimod-induced psoriasiform dermatitis in mice by mediating antiproliferative effects, Free Radical Research, 53(3), 269–280, doi:10.1080/10715762.2018.1564920, 2019.

Harrison, R. G.: Cloud Formation and the Possible Significance of Charge for Atmospheric Condensation and Ice Nuclei, Space Science Reviews, 94(1–2), 381–396, doi:10.1023/A:1026708415235, 2000.

Harrison, R. G. and Carslaw, K. S.: Ion-aerosol-cloud processes in the lower atmosphere, Reviews of Geophysics, 41(3), doi:10.1029/2002RG000114, 2003.

Hashino, T., Chiruta, M., Polzin, D., Kubicek, A. and Wang, P. K.: Numerical simulation of the flow fields around falling ice crystals with inclined orientation and the hydrodynamic torque, Atmospheric Research, 150, 79–96, doi:10.1016/j.atmosres.2014.07.003, 2014.

He, J., Hu, J., Liu, D. and Zhang, Y.-T.: Experimental and numerical study on the optimization of pulse-modulated radio-frequency discharges, Plasma Sources Sci. Technol., 22(3), 035008, doi:10.1088/0963-0252/22/3/035008, 2013.

Henin, S., Petit, Y., Kiselev, D., Kasparian, J. and Wolf, J.-P.: Contribution of water droplets to charge release by laser filaments in air, Appl. Phys. Lett., 95(9), 091107, doi:10.1063/1.3220066, 2009.

Hosseini, B. and Stockie, J. M.: Bayesian estimation of airborne fugitive emissions using a Gaussian plume model, Atmospheric Environment, 141, 122–138, doi:10.1016/j.atmosenv.2016.06.046, 2016.
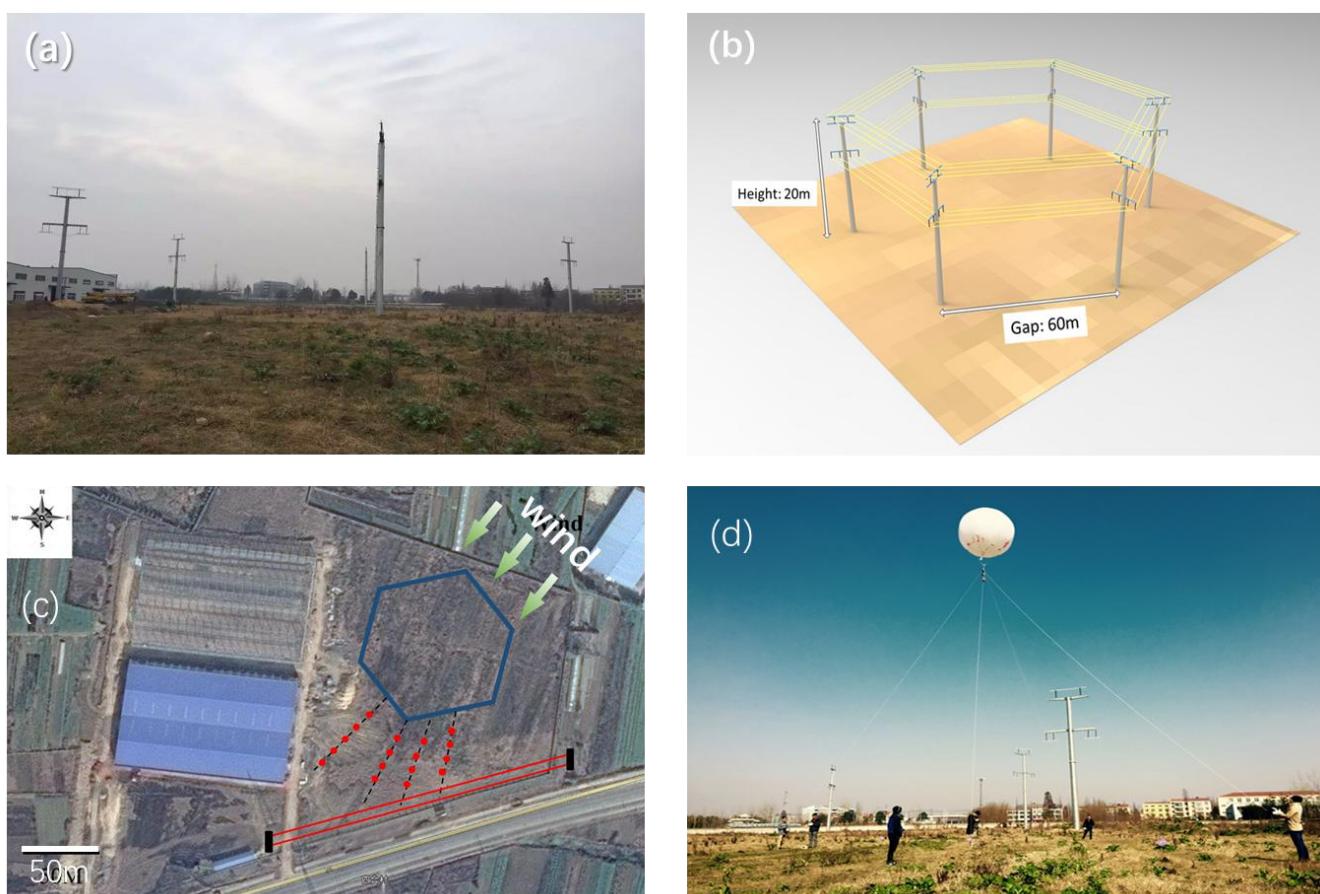
Hu, J. T., Liu, X. Y., Liu, J. H., Xiong, Z. L., Liu, D. W., Lu, X. P., Iza, F. and Kong, M. G.: The effect of applied electric field on pulsed radio frequency and pulsed direct current plasma jet array, Physics of Plasmas, 19(6), 063505-063505–5, doi:doi:10.1063/1.4729730, 2012.

Hu, J. T., Wang, J. G., Liu, X. Y., Liu, D. W., Lu, X. P., Shi, J. J. and Ostrikov, K.: Effect of a floating electrode on a plasma jet, Physics of Plasmas, 20(8), 083516-083516–5, doi:doi:10.1063/1.4817954, 2013.

Jidenko, N. and Borra, J. P.: Self-cleaning, maintenance-free aerosol filter by non-thermal plasma at atmospheric pressure, Journal of Hazardous Materials, 235–236, 237–245, doi:10.1016/j.jhazmat.2012.07.055, 2012.

Jolly, W. M., Cochrane, M. A., Freeborn, P. H., Holden, Z. A., Brown, T. J., Williamson, G. J. and Bowman, D. M. J. S.: Climate-induced variations in global wildfire danger from 1979 to 2013, Nat Commun, 6(1), 1–11, doi:10.1038/ncomms8537, 2015.

Keefe, D., Nolan, P. J. and Rich, T. A.: Charge Equilibrium in Aerosols According to the Boltzmann Law, Proceedings of the Royal Irish Academy. Section A: Mathematical and Physical Sciences, 60, 27–45, 1959.

Khain, A., Arkhipov, V., Pinsky, M., Feldman, Y. and Ryabov, Y.: Rain enhancement and fog elimination by seeding with charged droplets. part I: Ttheory and numerical simulations, J. Appl. Meteorol., 43(10), 1513–1529, doi:10.1175/JAM2131.1, 2004.

Lesk, C., Rowhani, P. and Ramankutty, N.: Influence of extreme weather disasters on global crop production, Nature, 529(7584), 84–87, doi:10.1038/nature16467, 2016.

Liu, J. H., Liu, X. Y., Hu, K., Liu, D. W., Lu, X. P., Iza, F. and Kong, M. G.: Plasma plume propagation characteristics of pulsed radio frequency plasma jet, Applied Physics Letters, 98, 151502, doi:10.1063/1.3573811, 2011.

Liu, X., Gan, L., Ma, M., Zhang, S., Liu, J., Chen, H., Liu, D. and Lu, X.: A comparative study on the transdermal penetration effect of gaseous and aqueous plasma reactive species, J. Phys. D: Appl. Phys., 51(7), 075401, doi:10.1088/1361-6463/aaa419, 2018.

Liu, X. Y., Hu, J. T., Liu, J. H., Xiong, Z. L., Liu, D. W., Lu, X. P. and Shi, J. J.: The discharge mode transition and O(5p1) production mechanism of pulsed radio frequency capacitively coupled plasma, Applied Physics Letters, 101(4), 043705-043705–4, doi:doi:10.1063/1.4733662, 2012.

Liu, X. Y., Pei, X. K., Lu, X. P. and Liu, D. W.: Numerical and experimental study on a pulsed-dc plasma jet, Plasma Sources Sci. Technol., 23(3), 035007, doi:10.1088/0963-0252/23/3/035007, 2014a.

Liu, X. Y., Pei, X. K., Ostrikov, K., Lu, X. P. and Liu, D. W.: The production mechanisms of OH radicals in a pulsed direct current plasma jet, Physics of Plasmas (1994-present), 21(9), 093513, doi:10.1063/1.4895496, 2014b.

Luan, T., Guo, X., Zhang, T. and Guo, L.: Below-Cloud Aerosol Scavenging by Different-Intensity Rains in Beijing City, J Meteorol Res, 33(1), 126–137, doi:10.1007/s13351-019-8079-0, 2019.

Mu, Y., Pang, X., Quan, J. and Zhang, X.: Atmospheric carbonyl compounds in Chinese background area: A remote mountain of the Qinghai-Tibetan Plateau, Journal of Geophysical Research: Atmospheres, 112(D22), doi:10.1029/2006JD008211, 2007.

Nielsen, J., Maus, C., Rzesanke, D. and Leisner, T.: Charge induced stability of water droplets in subsaturated environment, Atmospheric Chemistry and Physics, 11, doi:10.5194/acp-11-2031-2011, 2011.

Pan, S., Xu, M., Gan, L., Zhang, S., Chen, H., Liu, D., Li, Y. and Lu, X.: Plasma activated radix arnebiae oil as innovative antimicrobial and burn wound healing agent, J. Phys. D: Appl. Phys., 52(33), 335201, doi:10.1088/1361-6463/ab234c, 2019.

Pierce, J. R. and Adams, P. J.: Can cosmic rays affect cloud condensation nuclei by altering new particle formation rates?, Geophysical Research Letters, 36(9), doi:10.1029/2009GL037946, 2009.

Riba, J.-R., Morosini, A. and Capelli, F.: Comparative Study of AC and Positive and Negative DC Visual Corona for Sphere-Plane Gaps in Atmospheric Air, Energies, 11(10), 2671, doi:10.3390/en11102671, 2018.

Roy, A., Chatterjee, A., Ghosh, A., Das, S. K., Ghosh, S. K. and Raha, S.: Below-cloud scavenging of size-segregated aerosols and its effect on rainwater acidity and nutrient deposition: A long-term (2009-2018) and real-time observation over eastern Himalaya, Sci. Total Environ., 674, 223–233, doi:10.1016/j.scitotenv.2019.04.165, 2019.

Schleder, A. M. and Martins, M. R.: Experimental data and CFD performance for CO2 cloud dispersion analysis, Journal of Loss Prevention in the Process Industries, 43, 688–699, doi:10.1016/j.jlp.2016.03.027, 2016.

Shiyin, L., Wenxin, S., Yongping, S. and Gang, L.: Glacier changes since the Little Ice Age maximum in the western Qilian Shan, northwest China, and consequences of glacier runoff for water supply, Journal of Glaciology, 49(164), 117–124, doi:10.3189/172756503781830926, 2003.

Tan, X., Qiu, Y., Yang, Y., Liu, D., Lu, X. and Pan, Y.: Enhanced Growth of Single Droplet by Control of Equivalent Charge on Droplet, IEEE Transactions on Plasma Science, PP(99), 1–5, doi:10.1109/TPS.2016.2608832, 2016.

Tinsley, B. A. and Zhou, L.: Parameterization of aerosol scavenging due to atmospheric ionization, J. Geophys. Res.-Atmos., 120(16), 8389–8410, doi:10.1002/2014JD023016, 2015.

Trenberth, K. E., Dai, A., Schrier, G. van der, Jones, P. D., Barichivich, J., Briffa, K. R. and Sheffield, J.: Global warming and changes in drought, Nature Clim Change, 4(1), 17–22, doi:10.1038/nclimate2067, 2014.

Wang, J. G., Liu, X. Y., Liu, D. W., Lu, X. P. and Zhang, Y. T.: Mathematical model of gas plasma applied to chronic wounds, Physics of Plasmas (1994-present), 20(11), 113507, doi:10.1063/1.4826955, 2013.

Wang, P. K. and Pruppacher, H. R.: An Experimental Determination of the Efficiency with Which Aerosol Particles are Collected by Water Drops in Subsaturated Air, J. Atmos. Sci., 34(10), 1664–1669, doi:10.1175/1520-0469(1977)034<1664:AEDOTE>2.0.CO;2, 1977.

Yang, Y., Tan, X., Liu, D., Lu, X., Zhao, C., Lu, J. and Pan, Y.: Corona Discharge-Induced Rain and Snow Formation in Air, IEEE Trans. Plasma Sci., 46(5), 1786–1792, doi:10.1109/TPS.2018.2820200, 2018.

Yao, X., Jiang, N., Li, J., Lu, N., Shang, K. and Wu, Y.: An improved corona discharge ignited by oxide cathodes with high secondary electron emission for toluene degradation, Chem. Eng. J., 362, 339–348, doi:10.1016/j.cej.2018.12.151, 2019.

Zhang, B., He, J. and Ji, Y.: Prediction of average mobility of ions from corona discharge in air with respect to pressure, humidity and temperature, IEEE Trns. Dielectr. Electr. Insul., 26(5), 1403–1410, doi:10.1109/TDEI.2019.008001, 2019.

Zhang, L. and Tinsley, B. A.: Parameterization of aerosol scavenging due to atmospheric ionization under varying relative humidity, J. Geophys. Res.-Atmos., 122(10), 5330–5350, doi:10.1002/2016JD026255, 2017.

Zhang, L., Tinsley, B. A. and Zhou, L.: Parameterization of In-Cloud Aerosol Scavenging Due to Atmospheric Ionization: Part 3. Effects of Varying Droplet Radius, J. Geophys. Res.-Atmos., 123(18), 10546–10567, doi:10.1029/2018JD028840, 2018a.

Zhang, L., Tinsley, B. A. and Zhou, L.: Parameterization of In-Cloud Aerosol Scavenging Due to Atmospheric Ionization: Part 3. Effects of Varying Droplet Radius, J. Geophys. Res.-Atmos., 123(18), 10546–10567, doi:10.1029/2018JD028840, 2018b.

Zhou, X. and Yang, J.: A Novel Solar Thermal Power Plant with Floating Chimney Stiffened onto a Mountainside and Potential of the Power Generation in China's Deserts, Heat Transfer Engineering, doi:10.1080/01457630802414813, 2010.

Zou, X., Xu, M., Pan, S., Gan, L., Zhang, S., Chen, H., Liu, D., Lu, X. and Ostrikov, K. K.: Plasma Activated Oil: Fast Production,

Reactivity, Stability, and Wound Healing Application, ACS Biomater. Sci. Eng., 5(3), 1611–1622, doi:10.1021/acsbiomaterials.9b00125, 2019.


Figure 1. Large-scale installation for ion generation for precipitation of atmospheric aerosols, using over 300,000 corona plasma discharges. (a) The large-scale corona discharge system consists of 6 poles and 7.2 km electric wires. (b) The design diagram of the hexagonal discharge arrays. (c) The satellite image of the test zone (taken from https://map.baidu.com, last access: 29 December 2019). The hexagon shows the corona plasma discharge system. The red points show the locations of ion density measurements. (d) The hydrogen balloon carried the ion density measurement device.
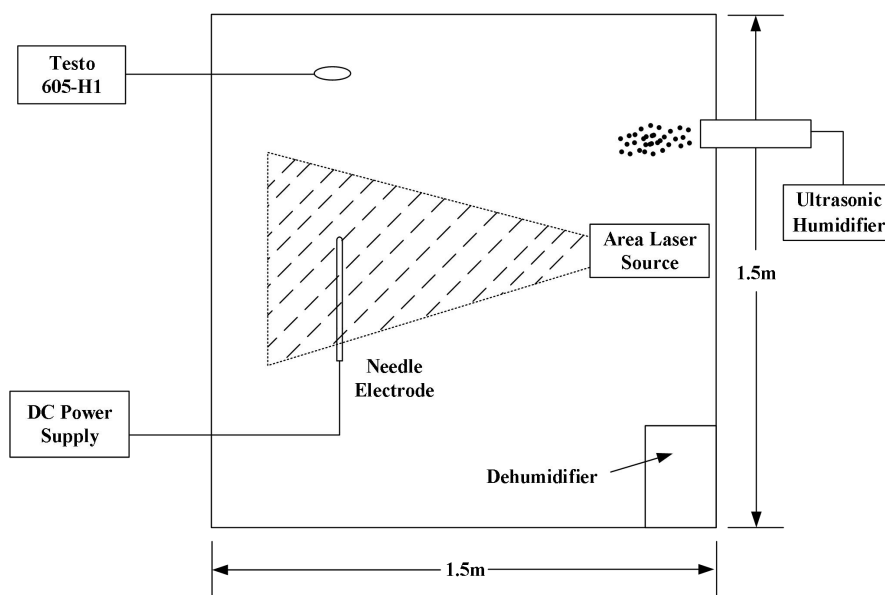
**Figure 2.** Schematic of the 6.75 m³ cloud chamber used for the ion-enhanced precipitation.
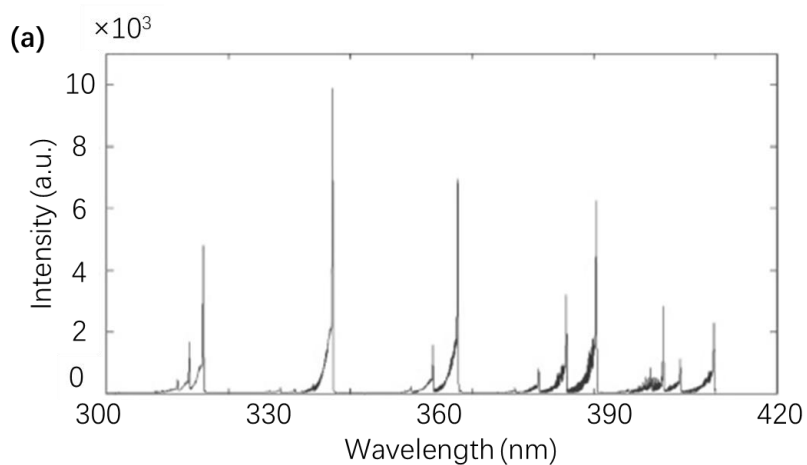
Figure 3. (a) Nitrogen species dominate the optical emission spectra (shown between 300 nm and 400 nm here) from the negative corona discharge on the wire electrode generated with the applied

voltage of -40 kV. (b) The image of corona discharge on the wire (1 m length, -40 kV). The exposure

time of the image is 0.5 seconds. The wire (diameter of 1 mm) was six strands of stranded wire.

(a)

(b)

(c) -30 kV   -60 kV   -90 kV

Max: 1.1×10^8 Max: 2.5×10^8 Max: 3.9×10^8
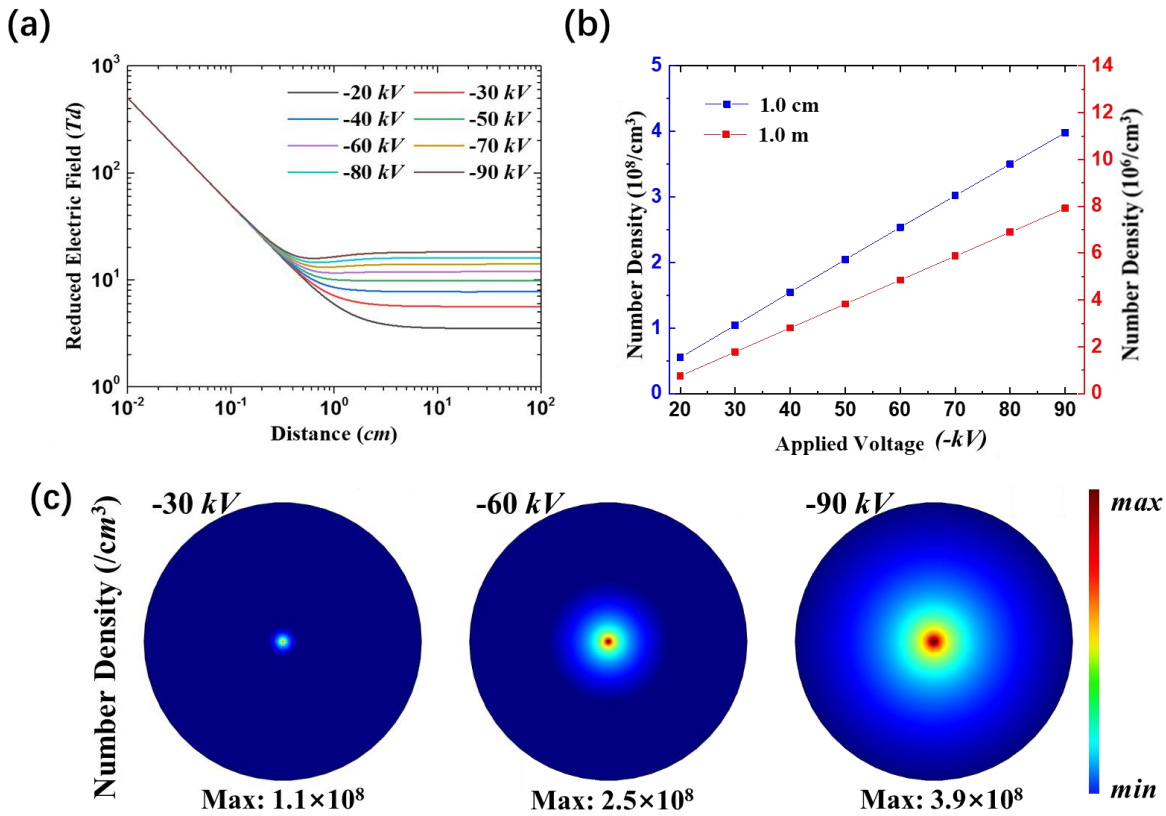
Figure 4. The increasing applied voltage enhances the ion output capacity of the corona discharge

source. (a) The electric field from the center as a function of applied voltage.(b) The ion density at 1

cm (blue line) and 1 m (red line) from the center as a function of applied voltage. (c) The distribution

of ions generated by single corona discharge point (simulation). The center is the corona discharge

point. The radius of the big blue circle is 1 m.
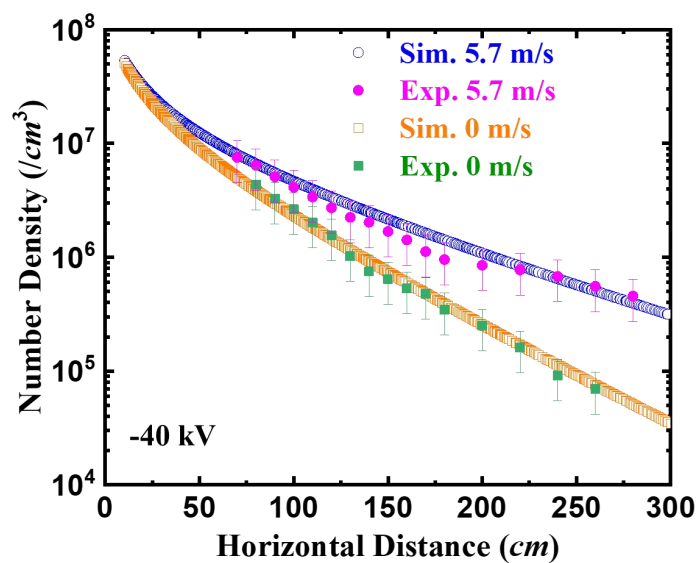
Figure 5. The effect of wind on the distribution of ions generated by a single corona discharge point (indoor tests). Wind speed at 0 m/s and 5.7 m/s. The applied voltage on the wire electrode was -40 kV. The experiment measurement data is plotted with error bars. The simulation data is plotted by hollow symbols.
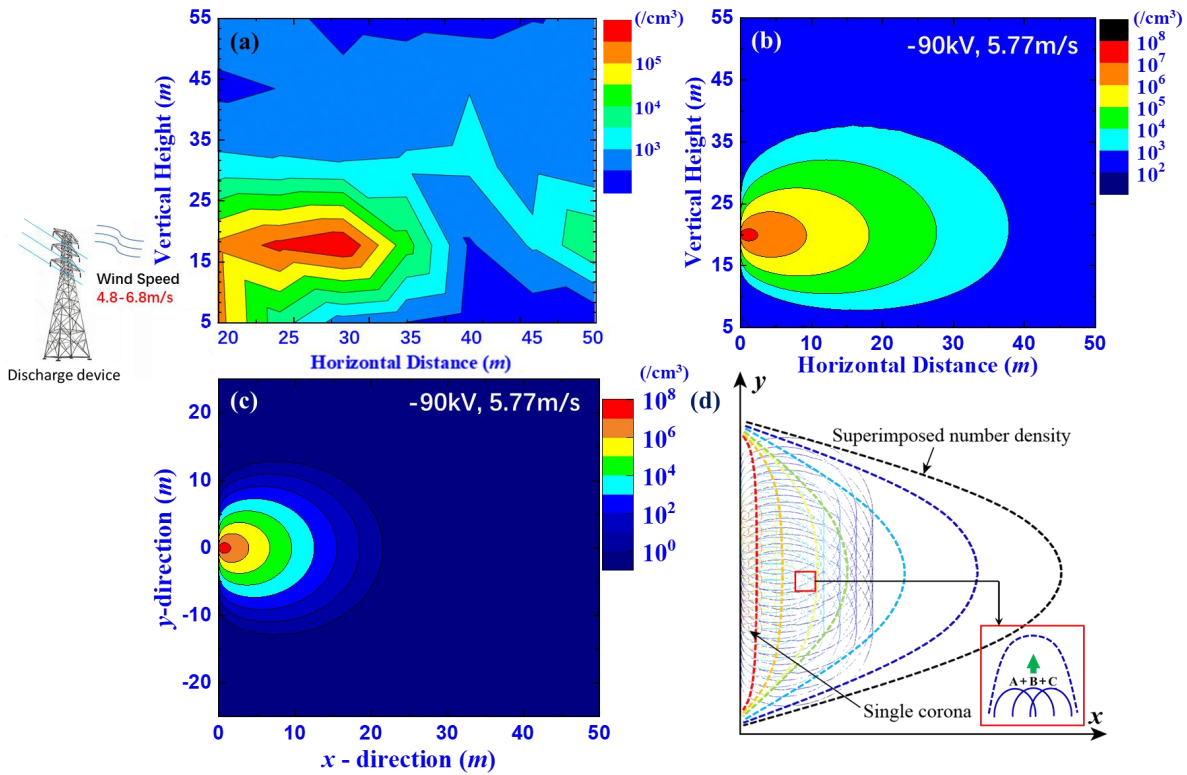
Figure 6. The coverage area of the large corona discharge system is the combination of the coverage areas of the very large number of corona discharge points. (a) The ion density distribution in vertical direction and downwind direction (experimental measurement, applied voltage -90 kV). (b) The ion density distribution in vertical direction and downwind direction (simulation, z axis (vertical direction), x axis (horizontal direction)). (c) The ion density distribution of single corona discharge point (-90 kV) in horizontal direction (x-y axis). (d) The combination of ions generated by multi-corona discharge points resulted in high negative ion density in the open air. The dashed color clines from red color to black color suggests the ion density decreases as the distance from the wire electrode increases. The inserted picture indicates the combination of ions generated by three corona discharge sources increases the coverage of ions substantially.
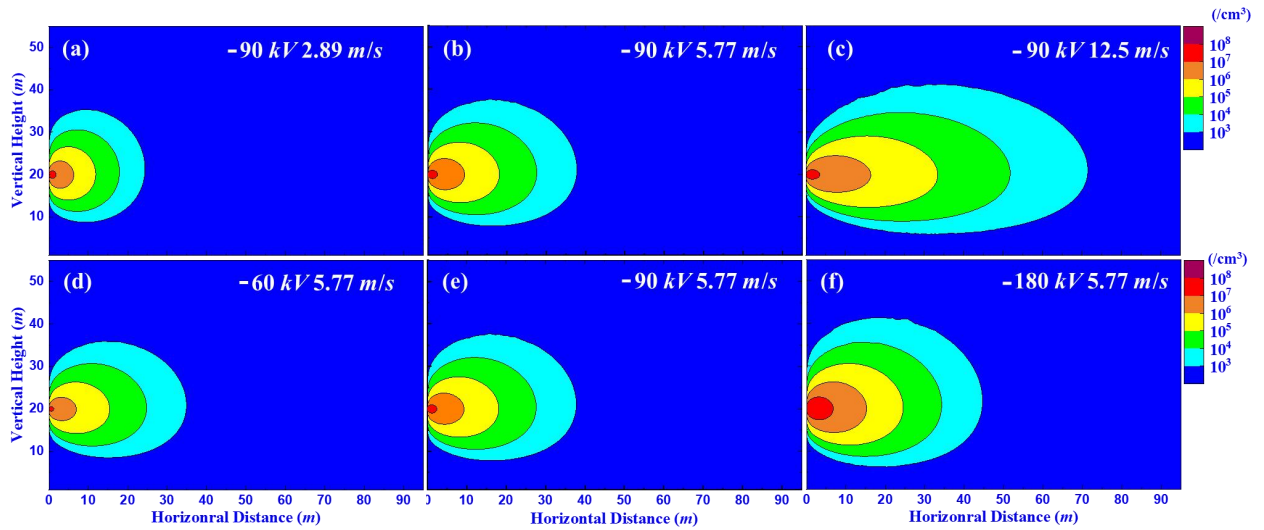
Figure 7. The increasing applied voltage and wind speed can enlarge the coverage area of the ion source. The effect of wind on the ion distribution in the field (numerical results). (a) -90kV, 2.89m/s (wind speed), (b)-90kV, 5.77m/s, (c)-90 kV, 12.5 m/s. The effect of wind on the ion distribution in the field (numerical results). (d) -60 kV. (e) -90 kV. (f) -180 kV.
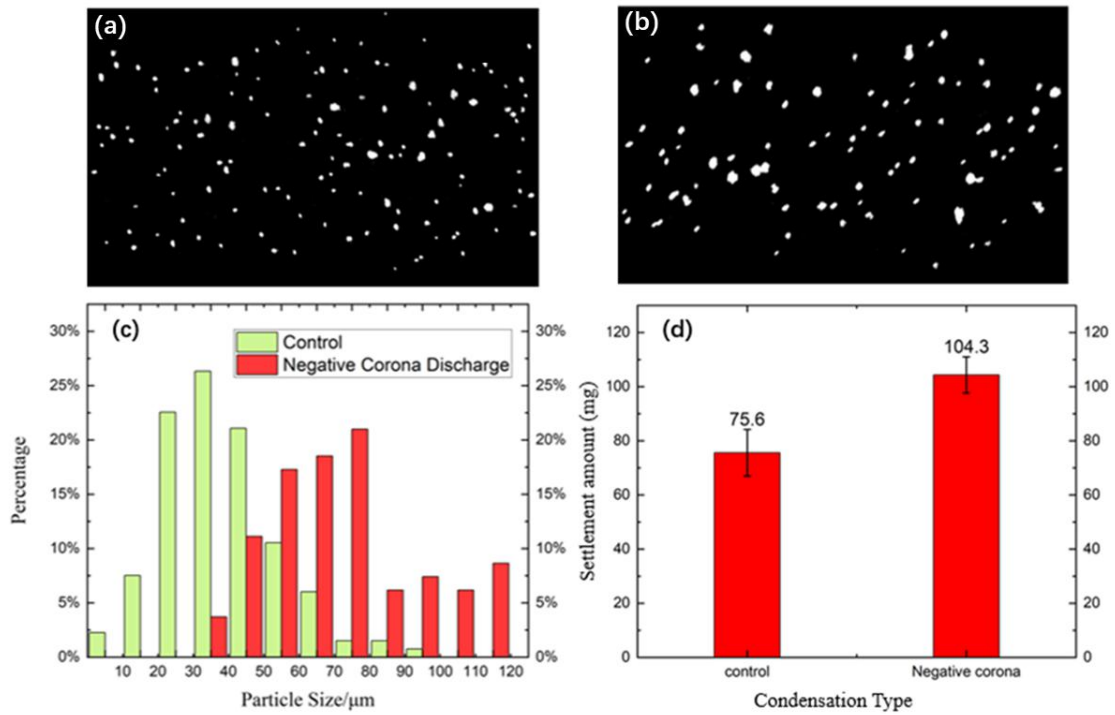
Figure 8. The ions generated by corona discharge source enhance the condensation of aerosols. The photo of aerosols in the light path of a laser for the case of (a) control group, (b) the enhanced condensation group by ions. The photo was taken 5 min after the experiment started. (c)The particle size distribution of aerosols in the cloud chamber for the control group and negative corona discharge group (calculated according to (a) and (b)). (d) The ions generated by corona discharge source enhance settlement of moisture. The settlement of moisture of control, negative corona discharge groups on the acceptor 10 min after the experiment started.